1-30-2024

Reactive Amine Functionalized Microelectrode Arrays Provide Short-Term Benefit but Long-Term Detriment to In Vivo Recording Performance

Lindsey N. Druschel
Case Western Reserve University, lnd24@case.edu

Pierce E. Boucher
Case Western Reserve University

George F. Hoeferlin
Case Western Reserve University, gfh16@case.edu

Dhariyat M. Menendez
Case Western Reserve University, dmm194@case.edu

Jonathan L. Duncan
Case Western Reserve University, jld155@case.edu

Recommended Citation

Brandon S. Sturgill, Ana G. Hernandez-Reynoso, Lindsey N. Druschel, Thomas J. Smith, Pierce E. Boucher, George F. Hoeferlin, Teresa Thuc Doan Thai, Madison S. Jiang, Jordan L. Hess, Neeha N. Alam, Dhariyat M. Menendez, Jonathan L. Duncan, Stuart F. Cogan, Joseph J. Pancrazio, and Jeffrey R. Capadona. Reactive Amine Functionalized Microelectrode Arrays Provide Short-Term Benefit but Long-Term Detriment to In Vivo Recording Performance. ACS Applied Bio Materials 2024 7 (2), 1052-1063. DOI: 10.1021/acsabm.3c01014

ACS APPLIED BIO MATERIALS

www.acsabm.org
Article

Reactive Amine Functionalized Microelectrode Arrays Provide Short-Term Benefit but Long-Term Detriment to *In Vivo* Recording Performance

Brandon S. Sturgill,[⊥] Ana G. Hernandez-Reynoso,[⊥] Lindsey N. Druschel, Thomas J. Smith, Pierce E. Boucher, George F. Hoeferlin, Teresa Thuc Doan Thai, Madison S. Jiang, Jordan L. Hess, Neeha N. Alam, Dhariyat M. Menendez, Jonathan L. Duncan, Stuart F. Cogan, Joseph J. Pancrazio,* and Jeffrey R. Capadona*

Cite This: *ACS Appl. Bio Mater.* 2024, 7, 1052−1063

ABSTRACT: Intracortical microelectrode arrays (MEAs) are used for recording neural signals. However, indwelling devices result in chronic neuroinflammation, which leads to decreased recording performance through degradation of the device and surrounding tissue. Coating the MEAs with bioactive molecules is being explored to mitigate neuroinflammation. Such approaches often require an intermediate functionalization step such as (3-aminopropyl)triethoxysilane (APTES), which serves as a linker. However, the standalone effect of this intermediate step has not been previously characterized. Here, we investigated the effect of coating MEAs with APTES by comparing APTES-coated to uncoated controls *in vivo* and *ex vivo*. First, we measured water contact angles between silicon uncoated and APTES-coated substrates to verify the hydrophilic characteristics of the APTES coating. Next, we implanted MEAs in the motor cortex (M1) of Sprague−Dawley rats with uncoated or APTES-coated devices. We assessed changes in the electrochemical impedance and neural recording performance over a chronic implantation period of 16 weeks. Additionally, histology and bulk gene expression were analyzed to understand further the reactive tissue changes arising from the coating. Results showed that APTES increased the hydrophilicity of the devices and decreased electrochemical impedance at 1 kHz. APTES coatings proved detrimental to the recording performance, as shown by a constant decay up to 16 weeks postimplantation. Bulk gene analysis showed differential changes in gene expression between groups that were inconclusive with regard to the long-term effect on neuronal tissue. Together, these results suggest that APTES coatings are ultimately detrimental to chronic neural recordings. Furthermore, interpretations of studies using APTES as a functionalization step should consider the potential consequences if the final functionalization step is incomplete.

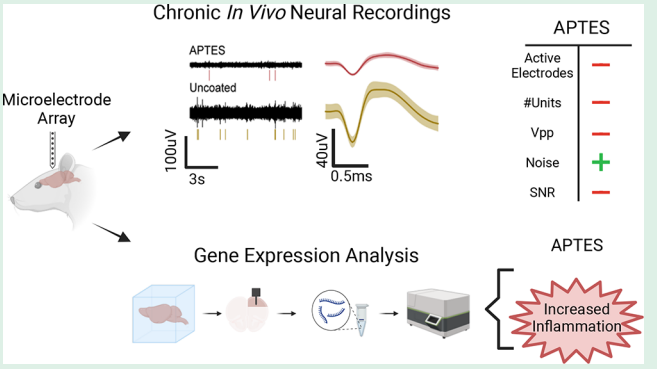

KEYWORDS: *coating, microelectrode arrays, motor cortex, neuroinflammation, surface modification*

1. INTRODUCTION

Intracortical microelectrode arrays (MEAs) offer a means of recording the extracellular bioelectric potentials of neurons for neuroprosthetic applications[1] or exploring the functional circuitry of the brain in healthy and diseased states.[2,3] These measured bioelectric potentials can reach up to several hundred microvolts and have a lower limit dictated by the recording channel noise.[4] While MEAs are often used for acute experiments, there is significant interest in devices capable of chronic recording for neuroprosthetic applications.[5] Unfortunately, the chronic use of commonly available MEA devices is limited by reduced recording performance or failure over implantation periods ranging from weeks to months, as characterized by a reduced number of single units detected and degrading signal quality.[6] The underlying basis for recording failure includes both degradation of device/material integrity, characterized by cracking of the insulation and delamination of conductive traces,[7,8] and a tissue response that exhibits features of neuroinflammation, characterized by glial scar formation, and oxidative stress that can lead to neuronal

Received: October 28, 2023
Revised: January 8, 2024
Accepted: January 10, 2024
Published: January 30, 2024

loss.[5,9] The goal of novel devices is to mitigate the tissue response and extend the recording performance.

Substantial efforts to develop new MEA architectures include devices with ultrathin shank dimensions or low modulus of elasticity materials to create flexible devices which aim to mitigate the tissue-device mechanical mismatch.[10−13] In addition, administration of pharmacological compounds postimplantation have been investigated including the use of dexamethasone,[14,15] resveratrol,[16] dimethyl fumarate,[17] and minocycline.[18] Several groups have recently explored the use of bioactive coatings, with the goal to mitigate neuroinflammation related to decreased chronic recording performance. For example, recent investigations have demonstrated improved chronic recording performance or decreased tissue response with coatings of dexamethasone loaded nitrocellulose,[19] laminin,[20] peptides,[21] neurotrophins loaded polypyrrole,[22] and antioxidants.[23,24] However, the silicon dioxide surfaces of MEAs may often require an intermediate functionalization step providing a more reactive surface for attaching bioactive molecules. For example, He et al. use polyethylenimine to functionalize the surface of planar silicon MEAs to initiate the self-assembly of laminin to the surface.[20] Alternatively, silane chemistries have been used in attaching the L1 neuro-adhesive molecule to silicon substrates used both in vitro and in vivo[25−27] and to attach an antioxidant compound to intracortical MEAs.[24,28] The organosilane (3-aminopropyl)triethoxysilane (APTES) is often used for this purpose.[25,29−31] APTES molecules form a self-assembled monolayer, which serves as a reactive linker for a range of bioactive molecules. This approach has been used to promote the attachment of antibodies on silicon dioxide-based chips,[32] acetylcholinesterase and choline oxidase onto carbon nanodots,[33] uricase enzyme onto indium tin oxide surfaces[34] bioactive peptides onto polyimide-insulated microwires,[21] extracellular matrix proteins on polydimethylsiloxane surfaces for neuronal culture,[35] glucose oxidase onto carbon nanotubes,[36] and synthetic antioxidants onto microelectrode arrays.[24] There is evidence that modification with APTES and other compounds with amine functional groups alone can promote cellular attachment and viability *in vitro* on materials including glass,[37] titanate nanotubes,[38] conducting polymer nanofibrous scaffolds,[39] silicon and silicon dioxide,[40−42] and the platinum electrodes of MEAs.[30,43] Interestingly, prior work suggests that there may be improved coupling, albeit acutely, of excitable cells to APTES-modified microelectrode sites such that recorded peak-to-peak amplitude reaches the mV range.[43,44] Although APTES and other silane coatings are being used as functionalization steps in these studies, their effect alone on neural recordings has not been characterized previously *in vivo*. This is particularly important depending on the type of molecule being conjugated to APTES functionalized substrates. For example, biologically derived molecules can be enzymatically degraded both *in vitro* and *in vivo*, which could result in the intermediate APTES functionalized substrate being the interface to biological cells and tissue.

The primary purpose of this study was to examine the effects of APTES coating on the recording performance of silicon-based laminar MEAs. Uncoated and APTES-coated silicon laminar MEAs were implanted within the rat motor cortex for periods that reached 16 weeks. Additionally, *in vivo* electrochemical impedance spectroscopy was performed to assess changes in the electrical properties of the device tissue interface.[45] Nonrecording laminar silicon probes were also implanted for additional shorter-duration studies focused on assessing the neuroinflammatory response to APTES-coated substrates. Post-mortem, brain tissue was harvested for either genomic evaluation of the neuroinflammatory response with a custom 152 gene panel. Our findings revealed a transient improvement in recording performance during the recordings performed on the day of surgery. However, after only 1 week *in vivo*, the improvements in the APTES group were lost and the recording performance at later time points quickly declined compared to controls. Post-mortem analysis of the neuroinflammatory response with gene expression analysis demonstrated a response that would not be promising for chronic neural recordings for either group, and thus was unable to provide correlative insight into the ability to maintain singly units recordings despite differential expression for several genes at a chronic time point.

2. MATERIALS AND METHODS

2.1. APTES Coating and Contact Angle Measurements. Square silicon tabs (1 cm × 1 cm, Catalog #1575, University Wafers, South Boston, MA, USA) and implantable MEAs were coated with APTES following previously described procedures.[24,46] Implantable MEAs used for this investigation were single-shank, 16-channel laminar silicon devices with silicon dioxide encapsulation (SiO_2), and a silicon substrate. Functional devices were purchased from NeuroNexus (A1 × 16−3−100−177-CM16LP, iridium electrode sites, NeuroNexus Technologies, Ann Arbor, MI, US). These devices were divided into two groups: (1) devices coated with APTES (n = 7) and (2) uncoated silicon devices acting as the untreated control (n = 8). In brief, square tabs and MEAs were first cleaned with 10 min rinses in the following exposure sequence: 1% Liquinox solution, deionized (DI) water (x2), acetone, methanol, and isopropyl alcohol. The square tabs and arrays were then further cleaned with UV ozone exposure for 18 min and then immediately transferred to a vacuum desiccator containing APTES in aqueous form. Then, a−74.5 kPa vacuum was created to enable gas phase deposition of APTES to the sample surfaces with the modifications detailed previously.[46]

Static contact angle measurements were taken on square tabs of silicon and APTES coated tabs to characterize the surface of each material and demonstrate the presence of APTES on the surface of our devices. Briefly, a drop of water (∼10 μL) was lowered onto either a silicon or APTES-coated square tab. A goniometer was used to measure the angle between the water drop and the substrate on both sides of the water droplet. Measurements for each drop were averaged between the two sides, and the measurements were repeated three times per surface condition to repeat a single value (mean ± SEM) for each substrate.

2.2. Animals and Surgical Implantation. Two cohorts of adult male Sprague−Dawley rats were used for this investigation. The first cohort (N = 15), approved by the University of Texas at Dallas Institutional Animal Care and Use Committee, involved the use of functional devices for single unit recordings. The second cohort (N = 9), approved by the Case Western Reserve University Institutional Animal Care and Use Committee, was used to assess the neuroinflammatory response using changes in inflammatory gene expression at 2 (n = 3), 7 (n = 3), or 11 weeks (n = 3) postimplantation. All animals were implanted with silicon nonfunctional probes. In this study, we focus on comparisons between the uncoated control versus APTES-coated probes.

For implantation of the first device cohort (functional devices), the surgical procedure was performed following established protocols.[6,47] Briefly, adult male rats (275−530 g) were anesthetized using vaporized isoflurane (1.8−2.2%) mixed with medical grade oxygen (500 mL/min; SomnoSuite for Mice & Rats, Kent Scientific Corporation, Torrington, CT, US). Following removal of scalp fur, animals were transferred onto a stereotaxic frame (David Kopf Instruments, Tujunga, CA, US). Vital signs were monitored throughout the entire surgery and recovery. The animal temperature

https://doi.org/10.1021/acsabm.3c01014
ACS Appl. Bio Mater. 2024, 7, 1052−1063

Table 1. Complete List of Neuroinflammatory and Oxidative Stress Genes of Interest Utilized in the Study[a]

Abl1	*C4a*	*Ddit3*	*Gsta1*	*Ins2*	*Ngfg*	*Prnp*	*Spp1*
Ager	*C5ar1*	*Dnm2*	*Gsta2*	*Ipcef1*	*Ngfr*	*Psen1*	*Src*
Aif1	*Casp3*	*Dock2*	*Gstm2*	*Irak4*	*Nme5*	*Psmb8*	*Srxn1*
Aim2	*Casp8*	*Ehd2*	*Gstp1*	*Irf7*	*Nol3*	*Ptgs2*	*Stx2*
Akt1	*Ccl1*	*Ep300*	*Gucy1b3*	*Itgam*	*Nos1*	*Ptpn6*	*Tbp*
Apoe	*Ccl5*	*Ercc6*	*H2-t23*	*Jun*	*Nos3*	*Ptx3*	*Tnf*
App	*Ccs*	*Erlec1*	*Hdac2*	*Keap1*	*Noxa1*	*Rela*	*Tnfrsf1a*
Arc	*Cd14*	*Fas*	*Hdac6*	*Lilrb4a*	*Nqo1*	*Rpl13a*	*Tnfrsf25*
Atf4	*Cd36*	*Fcer1g*	*Hgf*	*Lpo*	*Nr2f6*	*Rps18*	*Tor1a*
Atp13a2	*Cd45*	*Fcgr2b*	*Hif1a*	*Lrrk2*	*Nr4a2*	*Scd1*	*Tpm1*
Atp7a	*Cd68*	*Fn1*	*Hmox1*	*Mapt*	*Osgin1*	*Sdha*	*Trp53*
Atrn	*Cd74*	*Fos*	*Hprt*	*Mgmt*	*Osmr*	*Serpina3n*	*Trpm2*
Bad	*Cd84*	*Fxn*	*Hspb1*	*Mmp12*	*Oxr1*	*Sirt1*	*Txnl1*
Bcl2	*Cdk2*	*Gfap*	*Htra2*	*Mmp14*	*Park7*	*Sirt2*	*Txnrd1*
Bdnf	*Clec7a*	*Gnao1*	*Idh1*	*Mpeg1*	*Parp1*	*Slc8a1*	*Tyrobp*
Blnk	*Cln8*	*Gpr37*	*Il1b*	*Mutyh*	*Pdgfrb*	*Snca*	*Ubc*
Bnip3	*Ctss*	*Gsk3b*	*Il1r1*	*Ncf1*	*Pink1*	*Sod1*	*Ubqln1*
C3	*Cybb*	*Gsr*	*Il2rg*	*Nefh*	*Pla2g4a*	*Sod2*	*Vegfa*
C3ar1	*Cycs*	*Gss*	*Il6*	*Nfe2l2*	*Ppargc1a*	*Sod3*	*Xbp1*

[a]Here, we list the 152 genes examined in rat brain tissue in this study using a combination of custom genes (shown with light green shading) and preset genes from NanoString (unshaded). Housekeeping genes (used purely for normalization) are highlighted with light red shading.

was maintained using a far-infrared warming pad (PhysioSuite for Mice & Rats, Kent Scientific Corporation, Torrington, CT, US). Following cleaning of the scalp surgical site with alternating betadine and alcohol swabs, the surgical site was injected subcutaneously with 0.5% bupivacaine hydrochloride (Marcaine, Hospira, Lake Forest, IL, US). An incision was made at the midline of the scalp and the muscles and underlying connective tissue were removed. Two stainless steel 1.59 mm O.D. bone anchor screws (Stoelting Co., Wood Dale, IL, USA) were inserted into the skull to serve as ground and reference for electrophysiological and electrochemical measurements. A third screw was inserted for anchoring. A craniotomy of approximately 1 mm × 1 mm was performed over the right primary motor cortex (M1) region, followed by durotomy to allow for probe insertion. Craniotomy formation was performed under microscopic observation to minimize the likelihood of tissue injury and bleeding. Stainless steel reference and ground wires were wrapped around the two bone screws. Laminar silicon MEAs, either uncoated or APTES-functionalized were implanted targeting the motor cortex (M1) to a depth of 2 mm using a precision-controlled inserter at a rate of 1 mm/sec (NeuralGlider, Actuated Medical, Inc., Ann Arbor, MI, US). Care was taken to avoid rupture of surface blood vessels during insertion to minimize hemorrhaging. After insertion, a dural graft was placed around the probe (Biodesign Dural Graft, Cook Medical, Bloomington, IN, US) to cover the durotomy site, followed by a layer of tissue adhesive (GLUture, World Precision Instruments, Sarasota, FL, US) to seal the craniotomy site. A dental cement head cap was formed around the implant to secure the device to the skull. The incision was then closed using surgical staples and the animals were given 5 mg/kg intramuscular cefazolin (Med-Vet International, Mettawa, IL, US) as infection prophylaxis, and depending on availability either 1.2 mg/kg of subcutaneous slow-release buprenorphine (ZooPharm, LLC., Laramie, WY, US) or 1.3 mg/kg subcutaneous extended-release buprenorphine (Ethiqa XR, Fidelis Animal Health, North Brunswick, NJ, USA) for pain management every 72 h for 5 days. Animals were provided sulfamethoxazole and trimethoprim oral suspension (200 mg and 40 mg per 5 mL, Aurobindo Pharma, Dayton, NJ, US) in their drinking water (1 mL suspension/100 mL drinking water) for 1 week postimplantation.[6,24,47] For the second cohort, animals were prepared for surgery and device implantation, as detailed above. Craniotomies of approximately 1 mm × 1 mm were made ±3 mm lateral from midline and 2 mm anterior/posterior from bregma. Animals were then implanted with three nonfunctional laminar silicon probes that were uncoated or APTES-coated, or MnTBAP-coated (not directly related to the present study), each implanted randomly in different cortex regions as to not introduce confounding factors. The position of each of the implant types was varied to find a different craniotomy site in each animal. After insertion, the durotomy site was sealed with a layer of Kwik-Cast (World Precision Instruments, Sarasota, FL, US). A dental cement head cap was adhered to the implant and skull to ensure that the device remained secured. The incision was closed using sutures, and the animals were given 5 mg/kg intramuscular cefazolin (Med-Vet International, Mettawa, IL, US) as infection prophylaxis immediately after surgery and then again in the morning and evening 24 h after surgery. Animals were provided 1 mg/kg of subcutaneous meloxicam injection for pain management every 24 h for 2 days.

2.3. Electrochemical Impedance Spectroscopy. Electrochemical impedance spectroscopy (EIS) measurements were acquired (model 604E, CH Instruments, Bee Cave, TX, US) inside a Faraday Cage once per week in implanted anesthetized animals under 1.5−2.0% Isoflurane. Measurements were performed by driving a sinusoidal 10 mV RMS excitation voltage with respect to the grounding stainless steel bone screw to each electrode site independently while measuring the elicited current. The impedance

https://doi.org/10.1021/acsabm.3c01014
ACS Appl. Bio Mater. 2024, 7, 1052−1063

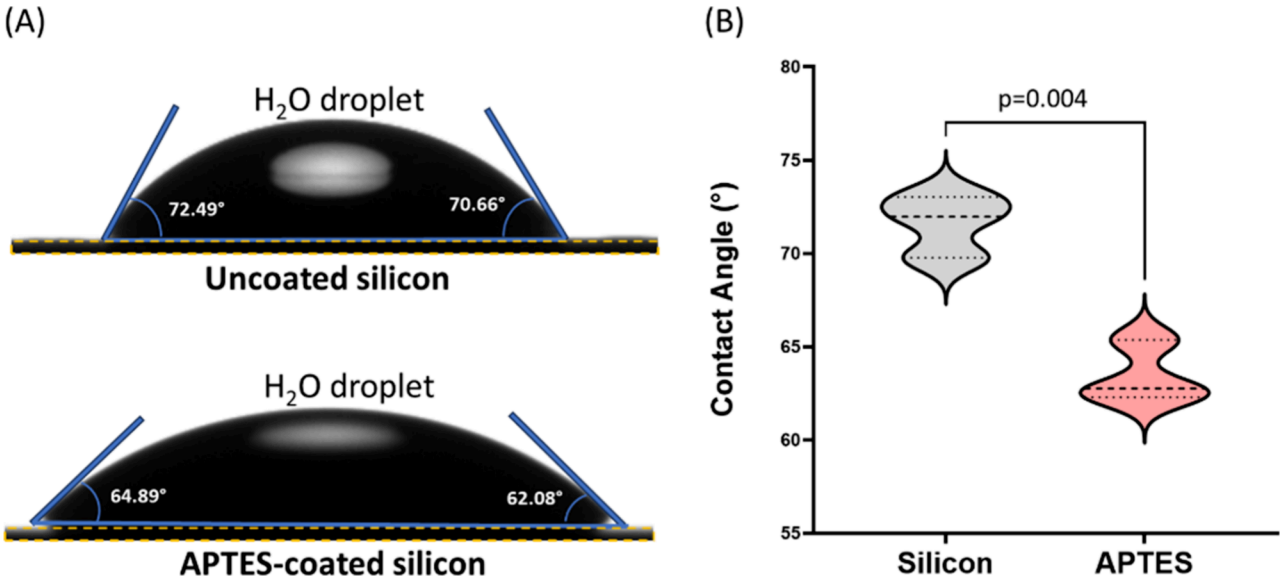

Figure 1. Static contact angle measurements for APTES and uncoated silicon tabs. (A) Representative images for the measurement of the contact angle of uncoated silicon (top) and APTES-coated (bottom) tabs. (B) Summary of contact angle measurements for multiple uncoated and APTES-coated substrates (N = 3). Violin plots represent the contact angle distribution for both groups showing the median (dashed line), and first and third quartiles (dotted lines).

spectra were acquired over a frequency range of 1 to 10^5 Hz with 12 points per decade.

2.4. Electrophysiological Recordings and Processing. Multichannel wideband data (0.1−7500 Hz) were collected (Omniplex, Plexon, Dallas, TX, US) at a sampling rate of 40 kHz per channel and recorded twice weekly for 10 min per session on lightly anesthetized animals using 1.7 to 2.1% isoflurane. Week 1 consists of recordings done on the day of implantation (day 0) and the first recording thereafter on day 7. Subsequent weeks are defined as spans of 7 days. Acquired data were processed using an Offline Sorter (OmniPlex Neural Recording Data Acquisition System, Plexon Inc., Dallas, TX, US). First, signals were band passed using a four-pole Butterworth filter with 300 and 3000 Hz cutoff frequencies, digitally referenced to the common averaged signal to reduce noise, and artifacts were removed by invalidation of signals appearing simultaneously on at least a third of recording channels. Single spikes were detected using a thresholding method, where voltage deflections of $4\sigma_{RMS}$ below the baseline mean were selected as putative neural activity. Single units were automatically sorted using a two-dimensional principal component space and K-means clustering, then manually validated. Performance metrics were then calculated using a custom MATLAB code (Mathworks, Natick, MA, US) to obtain the weekly proportion of active electrodes (electrode sites demonstrating single unit activity), number of units per electrode site, spike rate, voltage peak-to-peak amplitude (V_{pp}), noise levels, and signal-to-noise ratio (SNR) using equations shown in Table S1. The number of units per electrode site (eq S2) was calculated as the average number of single units recorded in a week for each nonexcluded electrode site. The spike rate (eq S3) was calculated as the inverse of the median interspike interval of each recorded unit in a week per electrode site. The V_{pp} (eq S4) was calculated as the sum of the peak and trough of the mean signal amplitude for units recorded at each electrode site. The noise level (eq S5) for each active channel was calculated by removing the spikes from the signal and reported as the RMS value. The SNR (eq S6) was calculated as the V_{pp} divided by the RMS noise on the corresponding active channel. Furthermore, values from multiple recordings during the week were averaged together and reported as the mean. Single electrode sites that did not record any single units throughout the entire duration of the study were excluded from the final analysis. Finally, to reduce week-to-week variations, which could be biological in nature, due to subtle differences in animal handling or timing of recording sessions, we proceeded to bin the data into three phases: acute (1−5 weeks), subchronic (6−11 weeks), and chronic (12−16 weeks), which largely overlap with previously reported progression of the neuroinflammatory cascade.[6,48]

2.5. Tissue Extraction for Gene Expression Analysis. For the second cohort, rats were euthanized at 2 weeks postimplantation (n = 3), 7 weeks postimplantation (n = 3), or 11 weeks postimplantation (n = 3). Animals were anesthetized with intraperitoneal injections of 160 mg/kg ketamine and 20 mg/kg xylazine. Once anesthetization was confirmed via a firm toe pinch, rats were transcardially perfused with 1× PBS followed by 30% sucrose in PBS. The volume of each solution varied between 400 and 800 mL based on weight. The brains were quickly explanted and placed in a mold filled with the optimal cutting temperature compound and frozen over dry ice to prepare for cryoslicing. The brains were stored at −80 °C until cryoslicing. The cryoslicing consisted of slicing eight 150 μm slices through the cerebral cortex. After each section was sliced, a 1 mm biopsy punch was taken over the electrode implantation sites. All eight biopsies of the implant sites were then pooled for each animal and collected in bead rupture tubes for homogenization.

2.6. RNA Isolation and Gene Expression Assessment. Homogenized samples were sent to the Gene Expression and Genotyping Facility at Case Western Reserve University for RNA isolation.[17,24,49] The RNeasy Plus Universal Mini Kit (Qiagen 73404) was used to isolate the RNA. Nanodrop and TapeStation systems were used to check the RNA quantity. Samples with concentrations too low for an nCounter run were concentrated by using a Speedvac. This isolated RNA was evaluated for the expression of 146 selected genes of interest, all known markers for oxidative stress or inflammation.[49−51] Additionally, six genes were selected as housekeeping genes for normalization (Table 1). The isolated RNA was hybridized with complementary sequences for RNA molecules of interest that were bound to a specific fluorescent sequence, known as a barcode. The hybridized samples were run through the nCounter MAX/FLEX system by NanoString Technologies, which scanned the samples and quantified the number of fluorescent barcode present. The instrument outputs the number of each fluorescent barcode scanned per sample, which corresponds to the number of each RNA of interest found in each sample.

2.7. Statistical Analysis. RStudio (2023.06.1 + 524, PBC, Boston, MA, US) was used to prepare data for statistical analysis using a custom script. Microsoft Excel (Microsoft Corporation, Redmon, WA, US) was used to calculate a two-sample test of

https://doi.org/10.1021/acsabm.3c01014
ACS Appl. Bio Mater. 2024, 7, 1052−1063

proportions to compare the proportion of active electrodes between groups. GraphPad Prism 10 (Version 10.0.2(232) Dotmatics, Boston, MA, US) was used to calculate the statistical analysis as following: a Shapiro–Wilk test for normality was conducted to determine normal distribution of data. Linear regression was calculated for the impedance magnitude and the proportion of active electrodes of both groups using a least-squares linear regression in GraphPad Prism with outlier removal using a Robust regression and Outlier removal methodology with a $Q = 1\%$.[52] The slope for each group was then tested to determine statistical difference from zero using an F-test and further tested between groups. Then, the slopes of both groups were compared to each other to determine statistical differences. We further stratified the proportion of active electrodes to account for depth differences. We grouped electrodes on lamina L2/3 and L4 of the motor cortex and labeled as superficial, lamina L5 as middle, and L6 as deep. For non-normally distributed neurophysiological and electrochemical measurements, a Kruskal–Wallis test followed by a posthoc Benjamini–Krieger–Yekutieli test to adjust for multiple comparisons, in order to determine differences between groups at all time points. For contact angle measurements, an unpaired, two-tailed parametric t test was conducted to compare uncoated silicon and APTES-coated surfaces in GraphPad Prism 9.4.1. Unless otherwise stated, all data are represented as mean ± standard error of the mean (SEM). In all cases, $p < 0.05$ was considered as statistically significant.

Gene expression data was analyzed using the nSolver software provided by NanoString Technologies. This software inputs the raw counts from the instrument and allows for normalization, thresholding, ratio calculations, and t tests. First, samples were normalized using both positive control probes and housekeeping genes to account for the efficacy of hybridization and the amount of RNA collected. Genes with fewer than 20 counts in 85% of the samples were removed. A 2-tailed, unequal variance t test was performed for each gene and results were visualized on volcano plots. A Benjamini–Hochberg correction using a false discovery rate of 0.2 was used to filter out random significance due to the large number of genes evaluated in this study. Data were visualized by using volcano plots generated in GraphPad Prism 10.

3. RESULTS AND DISCUSSION

3.1. Contact Angle and Electrochemistry. To characterize the effects of surface modification by APTES, static contact angle measurements were taken from square tabs of silicon and APTES. Figure 1A shows representative images captured from contact angle measurements for APTES-coated and uncoated silicon substrates. A change in contact angle was observed after APTES coating (Figure 1B), which was found to be statistically significant ($p = 0.004$; unpaired, two-tailed parametric Student's t test); APTES-coated surfaces demonstrated a contact angle of 63.48 ± 1.65° (mean ± SEM, − = 3 samples), whereas uncoated substrates showed a contact angle of 71.59 ± 1.67° ($n = 3$ samples). These results are consistent with prior work demonstrating APTES functionalization slightly increases the hydrophilicity of the substrate.[29,30] The APTES group introduces a more reactive chemistry, which can be utilized to further functionalize the substrates.

3.2. Electrochemical Characterization of Functional MEAs. Electrochemical impedance spectroscopy was performed to assess changes at the neural interface after implantation throughout the duration of the study. Figure 2A shows representative measurements of impedance magnitude taken from the same individual electrode site at 3, 9, and 16 weeks postimplantation. The impedance magnitude for the overall spectra (e.g., 1 to 10^5 Hz) appeared to be lower for the APTES group compared to uncoated controls. Statistical analysis of the impedance magnitude at 1 kHz (Figure 2B) confirmed these observations. Initially, the

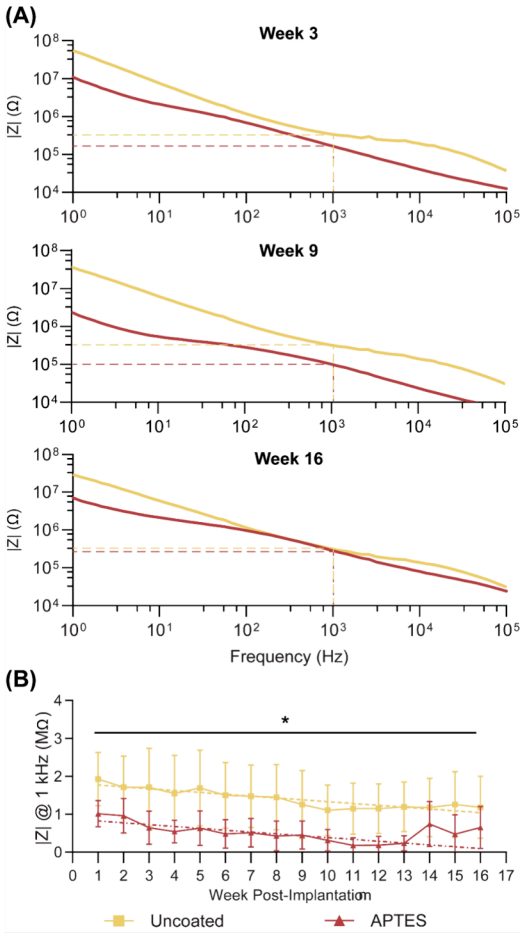

Figure 2. *In vivo* electrochemical impedance spectroscopy for APTES-coated and uncoated control devices. (A) Representative impedance magnitude for individual electrode sites at weeks 3, 9, and 16 post implantation; dashed lines indicate the impedance magnitude at 1 kHz. (B) Quantification of 1 kHz impedance magnitude for all weeks postimplantation with linear regression line. Data are shown as mean ± SD * $p < 0.05$; the horizontal bar on quantification plots indicates that all time points underneath were found to be statistically significant between groups.

uncoated devices had an impedance magnitude of 1.92 ± 0.17 MΩ, while APTES-coated devices showed 1.01 ± 0.04 MΩ ($p = 0.007$). Our findings are consistent with prior work by Wolf et al.[30] which has demonstrated that APTES coatings of platinum electrodes produced a small reduction in impedance magnitude across a wide frequency range, mainly due to an increase in effective capacitance for APTES coated sites. Additionally, linear regressions were used to evaluate time dependent changes. Linear regression analysis to impedance magnitude of both groups devices showed a consistent decline (APTES: $y = -0.05x + 0.9$, $R^2 = 0.69$; uncoated: $y = -0.05x + 1.8$, $R^2 = 0.81$; difference in slope between groups $p = 0.98$) with week-to-week variations that may be related to data collection. This confirms that slopes of decrease are similar between groups. Furthermore, changes in the electrochemical impedance spectrum after implantation show a decrease for all frequencies. This type of magnitude decrease has been observed in previous investigations normally after a few weeks postimplantation.[24,53] While there may be a biological contribution to the decreases, it is also possible that it may be due to leakage pathways on the probe as well as

https://doi.org/10.1021/acsabm.3c01014
ACS Appl. Bio Mater. 2024, 7, 1052–1063

back-end circuit bonds and interconnects. Though the offset between groups was found to be statistically significant, both were within impedance magnitude levels known to achieve high-quality recording of single unit activity, and thus do not represent substantial functional differences.[54]

3.3. Electrophysiological Recordings. The present study has examined, for the first time, to the best of our knowledge, the *in vivo* effect of APTES coating on implanted MEA performance and surrounding tissue response in the rat motor cortex. Our study primarily demonstrates that the APTES coating can acutely improve extracellular recording from silicon probes *in vivo* as shown by statistically significant increases in both proportion of active electrodes and Vpp for APTES-coated devices under acute recording conditions. However, the coating seemed to have only a short-lived benefit and appeared to be deleterious under chronic recording conditions. This interpretation is largely supported by a decrease in the proportion of active electrodes over time and a statistically significant reduction after week 11 *in vivo*.

Qualitative observations of both uncoated and APTES devices demonstrated the ability to record spontaneous single unit activity from anesthetized animals after implantation (Figure 3A) and up to at least 9 weeks postimplantation (Figure 3B). However, during later time points (Figure 3C), the number of resolvable single units, and recording quality from APTES devices decreased significantly, as shown by a reduction in the proportion of active electrodes and a decrease in the number of units, the V_{pp}, and the overall SNR (Figures 3C and 4). In contrast, uncoated controls appeared to have a declining, yet more stable signal quality after implantation. These results suggest a negative effect of the APTES coating that is detrimental to neuronal function. We then proceeded to quantify the proportion of active electrodes and the quality of the signal for the duration of the implantation period. Electrode sites that did not record a single unit for the entire duration of the study we excluded, resulting in no significant differences between groups ($p = 0.30$); with an average of 1.1 ± 0.5 electrode sites excluded for APTES MEAs and 2.0 ± 0.6 electrode sites excluded for uncoated MEAs.

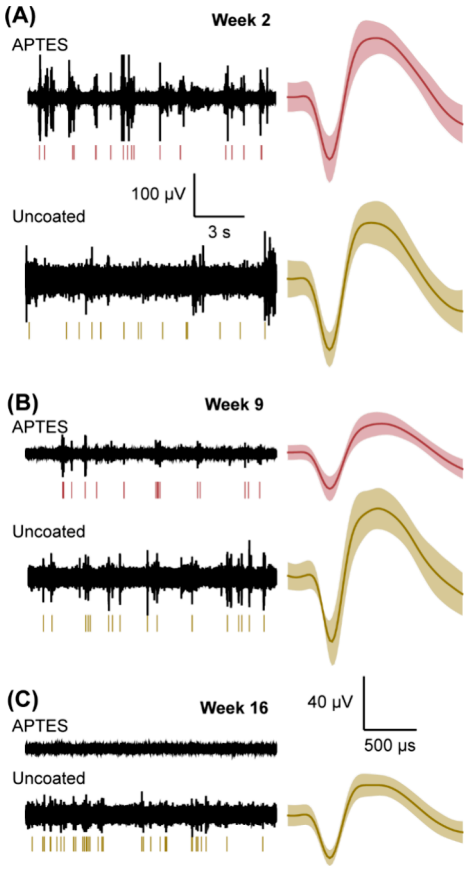

Figure 3. *In vivo* neural recordings of APTES and uncoated devices. Examples of continuous recordings of filtered data (left), raster plots (bottom) highlighting occurrence of spikes, and single units (left) for single electrode sites at 2 (A), 9 (B), and 16 (C) weeks post implantation. Representative single units are shown as mean ± SD.

Quantification revealed significant differences in the proportion of active electrodes between uncoated and APTES-coated MEAs (Figure 4A). The proportion of active electrodes for uncoated control devices started at 55% on the day of surgery and increased to 80% after a week of recovery. However, it decreased thereafter between weeks 2 and 7 where it appears to stabilize between 51 and 58% until 15 weeks. Linear regression analysis further confirmed this observation ($y = -0.6x + 63.7$; $R^2 = 0.14$). In contrast, the APTES-coated devices exhibited a significantly higher proportion of active electrodes on the day of surgery compared to uncoated devices (85% for APTES vs 55% for uncoated, $p < 0.0001$). However, unlike uncoated, the APTES-coated devices did not increase after 1 week of recovery. APTES-coated devices showed an overall quick and steady decline between weeks 2 (proportion: 77%) and 16 (proportion: 19%) with transient week-to-week variations. Linear regression confirmed these observations ($y = -3.8x + 80.6$; $R^2 = 0.91$). No statistical differences ($p > 0.05$) were found between APTES-coated and uncoated devices during 2 and 11 weeks postimplantation. However, differences were noted between the two groups again from week 12 to week 16 ($p < 0.01$) when the APTES devices reached a proportion of active electrodes of 38% and continued to decline to 19%. Additionally, the slopes of the linear regressions between the two groups were significantly different ($p < 0.0001$) which further confirms that APTES coated resulted in a decreased performance over time.

Depth analysis (Figure S1) revealed that the deep layer (L6) had the lowest proportion of active electrodes throughout the implantation period. A negative slope is observed for the APTES devices for superficial ($y = -0.6x + 87.1$; $R^2 = 0.05$), middle ($y = -4.2x + 95.2$; $R^2 = 0.86$), and deep ($y = -1.8x + 47.9$; $R^2 = 0.0.57$) layers. Similarly, a negative slope was observed for the uncoated devices for superficial ($y = -1.5x + 62.8$; $R^2 = 0.41$; slope comparison between APTES and uncoated, $p = 0.29$) and middle ($y = -0.5x + 78.2$; $R^2 = 0.06$; slope comparison between APTES and uncoated, $p < 0.0001$) but not for deep ($y = -0.3x + 34.8$; $R^2 = 0.05$; slope comparison between APTES and uncoated, $p = 0.0006$) layers. These results suggest that the APTES proportion of active electrodes decreases significantly for most depths of implantation. The decrease proportion of active electrodes in deep layers may be due to less neuronal cell density associated with L6.[55] Additionally, results of the control devices are similar to the results in deep layers seen from antioxidant coated devices in a previous study.[24] This further demonstrates the decreased performance of APTES coated devices over time compared to that of uncoated devices.

Similarly, the average number of units recorded per electrode site (Figure 4B) was found to follow the same

https://doi.org/10.1021/acsabm.3c01014
ACS Appl. Bio Mater. 2024, 7, 1052−1063

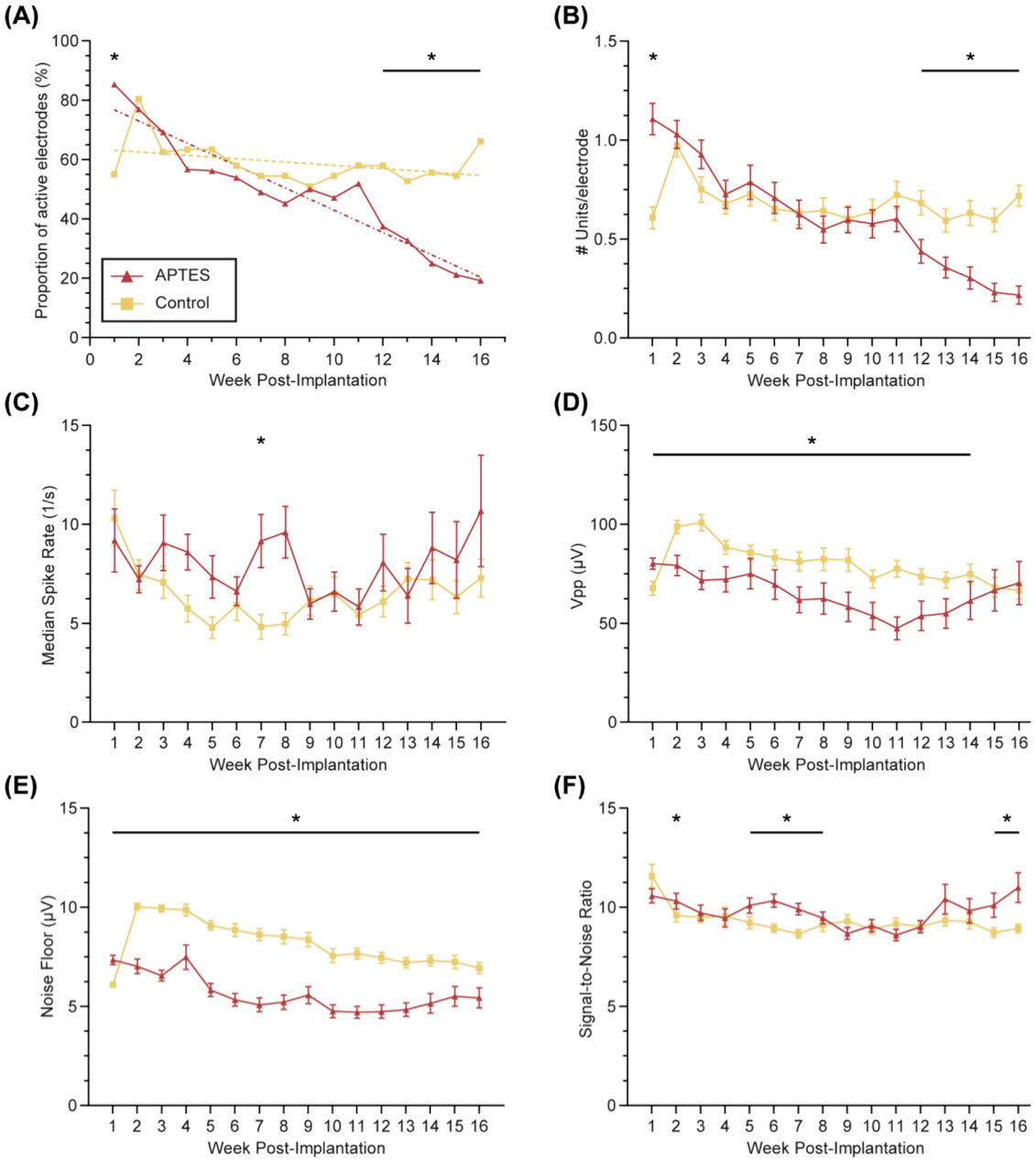

Figure 4. Quantification of APTES-coated and uncoated intracortical MEA recordings. (A) Proportion of active electrodes recording single units up to 16 weeks post implantation with linear regression, (B) average number of single units per electrode site, (C) median spike rate, (D) voltage peak-to-peak, (E) RMS noise floor, and (F) signal-to-noise ratio. Data is shown as mean ± SEM where applicable. Significance level: * $p < 0.05$. Single line with asterisk over multiple weeks indicates statistical differences during each week underlined.

trends as the proportion of active electrodes, with statistical differences between groups at weeks 1 (APTES: 1.11 ± 0.08 and uncoated: 0.61 ± 0.05 units per electrode) and 12 to 16 (APTES: ± and uncoated: 0.75 ± 0.06 units per electrode). Binning of the data into acute, subchronic, and chronic periods (Figure S2A) confirmed these observations, where the only statistical differences were found in the chronic period (APTES: 25%, and uncoated: 58%; $p < 0.0001$); however, the binned average number of units detected per electrode (Figure S2B) was significantly higher for APTES-coated devices during the acute period ($p = 0.004$) comparable during the subchronic ($p = 0.09$) and lower units during the chronic ($p < 0.0001$). Furthermore, the APTES coating did not appear to have a significant effect on the median spike rate of recorded units (Figure 4C and Figure S2C). These results suggest that APTES-coated probes may have a high proportion of active electrodes upon implantation; however, this effect is short-lived, and the coating appears detrimental to the chronic recording performance of intracortical MEAs.

The acute benefit of the APTES-coating was not limited to the proportion of active electrodes and average number of recorded units but presented differences in the quality of recorded signals (Figure 4D−F and Figure S2D-F; all variables were not normally distributed). We observed that APTES-coated MEAs had significantly higher V_{pp} upon implantation (80.2 ± 2.8 μV vs uncoated: 67.7 ± 3.5 μV; $p = 0.01$), but the signal quickly degraded between weeks 2 (79.2 ± 5.1 μV) to 14 (61.5 ± 9.5 μV) finalizing at 70.3 ± 10.9 μV at week 16,

https://doi.org/10.1021/acsabm.3c01014
ACS Appl. Bio Mater. 2024, 7, 1052−1063

while uncoated controls had a sudden increase at week 2 (98.8 ± 3.3 μV; $p < 0.001$) followed by a V_{pp} decrease until the end of the implantation period (66.5 ± 4.3 μV; $p = 0.44$). Binned analysis confirmed these observations, resulting in statistically significant differences between groups during the acute ($p = 0.0004$), subchronic ($p < 0.0001$), and chronic ($p = 0.002$) periods. We observed that RMS noise levels from uncoated control devices (6.1 ± 0.9 μV) were significantly lower than APTES-coated devices (7.34 ± 0.23 μV; $p = 0.0005$) on the day of surgery. However, at week 2, noise floor levels were higher in RMS amplitude for uncoated controls (10.0 ± 0.2 μV) than APTES-coated MEAs (7.0 ± 0.4 μV, $p < 0.0001$) (Figure 4C). The noise floor level of uncoated control devices decreased consistently through the study ending at 6.9 ± 0.3 μV, while the noise levels for APTES-coated devices consistently decreased until week 10 (4.8 ± 0.3 μV) when they became stable around 5 μV RMS and ended at 5.4 ± 0.5 μV at week 16. From week 2 to the end of the study, noise floor levels remained significantly lower for the APTES group than the control group ($p < 0.01$). The V_{pp} and RMS noise floor resulted in comparable ($p = 0.43$) SNR on the day of surgery between uncoated control devices (11.57 ± 0.59) and APTES-coated devices (10.57 ± 0.36). The SNR at active electrode sites of APTES-coated devices was statistically higher at week 2 ($p = 0.02$), weeks 5−8 ($p < 0.05$), and weeks 15−16 ($p < 0.05$). This was likely driven by the significantly lower noise levels observed with APTES devices. However, we observed week-to-week variability that resulted in statistically significant differences between groups. These week-to-week differences may be attributable to uncontrolled experimental variables perhaps biological in nature or due to subtle differences in animal handling. Because of this, binned analysis was conducted to reduce this variability by accounting for repeated measures. Binned results confirmed these results with statistical differences ($p < 0.01$) between groups during the acute, sub chronic, and chronic periods for V_{pp} and noise, resulting in higher SNR only during the chronic period ($p = 0.04$).

Overall, these results suggest that the APTES coating may improve signal quality acutely but not chronically. These changes may be due to a positively charged surface, known to promote nonspecific cell adhesion provided by the amine groups of APTES exposed to the surface of the coating.[56] APTES has demonstrated the ability to promote cell adhesion and increase cell-surface mechanical coupling *in vitro*.[30,43] Additionally, significant increases in the signal amplitudes recorded from rat cortical neurons and cardiomyocyte cells *in vitro* have been attributed to the enhanced cell-surface coupling and a resulting an increase in seal impedance.[30,43] However, the enhanced coupling also led to an increase in cell death after 9 days.[30] These observations are consistent with our results for the recordings acquired on the day of surgery with an increased V_{pp} for the APTES-coated devices, although the magnitude of signal enhancement for our *in vivo* measurements appeared to be far less than that observed for the *in vitro* studies. However, after implantation of APTES-coated devices, we observed a quick decline of approximately 40% the V_{pp} during the first 11 weeks postimplantation, followed by a transient recovery at the end of the study, while uncoated controls showed a more stable response throughout the implantation period. Interestingly, the noise levels were lower for the APTES-coated MEAs throughout all 16 weeks postimplantation except for the day of surgery. It is important to note that while the V_{pp} for the APTES-coated devices is lower than the uncoated controls, the noise levels were lower for the APTES-coated MEAs throughout all 16 weeks postimplantation except for the day of surgery. Concurrently, noise levels were observed to be lower, resulting in comparable signal-to-noise ratios between the APTES-coated MEAs and uncoated controls for almost all weeks postimplantation. We hypothesize that these differences may arise from the positively charged amine group of APTES that promotes nonspecific cell adhesion.[56] Furthermore, the constant loss in the proportion of active electrodes able to record single units throughout the 16 weeks postimplantation suggests a loss in neuronal function as a direct result of the APTES coating. These results may be explained by the increased cellular adhesion that, *in vivo*, applies not only to neurons but to the reacting glial cells as well, which may exacerbate glial scarring and oxidative stress, leading to neuronal loss.

Overall, these results suggest that the APTES coating may improve initial signal quality, possibly due to greater cell adhesion on APTES coated probes increasing the seal resistance as suggested by Wolf et al.[30] but the loss of neuronal signal overtime discourages its use as a final coating for *in vivo* studies and supports it only as an intermediate functionalization step to achieve adherence of other bioactive coatings.

3.4. Neuroinflammatory Gene Expression. Evaluation of 152 genes associated with neuroinflammation and oxidative stress was performed to evaluate the tissue response. Animals from this second cohort were quantitatively assessed for neuroinflammatory gene expression at 2, 7, and 11 weeks postimplant. We chose to examine the gene expression at 2, 7, and 11 weeks postimplant because these time points span the acute (2 weeks), subchronic (7 weeks), and transition to chronic (11 weeks). The chronic phase is generally stated at 12 weeks, but gene expression precludes protein expression and phenotypic changes. At both 2 and 7 weeks postimplantation, we found no significant difference in the neuroinflammatory gene expression between the tissue adjacent the APTES-coated probes and the uncoated control probes (data not shown). However, at 11 weeks postimplantation, we found seven differentially expressed genes in the comparison between the inflammatory response to control implants and APTES-coated implants (Figure 5). More specifically, two genes were differentially upregulated in the APTES-coated group compared to the control group: brain-derived neurotrophic factor (*Bdnf*) and histone deacetylase 6 (*Hdac6*). *Bdnf* encodes for a member of the nerve growth factor family of proteins. Binding of *Bdnf* proteins to their coordinating receptors has been shown to promote neuronal survival.[57] *Hdac6* is associated with transcriptional regulation and progression through cell cycle/development.[58] Since the results are not cell specific, it remains unclear if the upregulation of Hdac6 would be pro- or anti-inflammatory in nature. Additionally, five genes were differentially increased in the control group compared with the APTES-coated implants: endoplasmic reticulum lectin 1(*ERLEC1*), transmembrane ER and ERGIC protein (*Cln8*), G protein-coupled receptor 37 (*Gpr37*), glutathione *S*-transferase Pi 1 (*Gstp1*), and sirtuin 2 (*Sirt2*). *ERLEC1* functions as a regulator of multiple cellular stress-response pathways in a manner that promotes metastatic cell survival.[59] *Cln8* plays a role in cell proliferation during neuronal differentiation and in protection against cell death.[60] However, *Gpr37* encodes for a receptor for neuroprotective and glio-

https://doi.org/10.1021/acsabm.3c01014
ACS Appl. Bio Mater. 2024, 7, 1052−1063

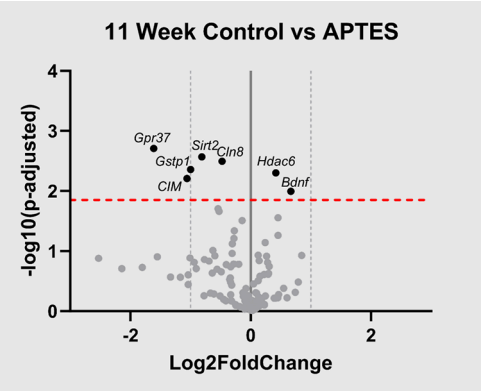

Figure 5. Bulk gene analysis tissue isolated adjacent to the implant site. Custom gene panels examined the differential expression of 152 oxidative stress and neuroinflammatory genes associated with neural implants. Log2(fold change) is based on differential expression between pairs of Control vs APTES coated, at 2, 7, or 11 weeks postimplantation with a 2-tailed unequal variance *t* test for each gene. Combinations not visualized in this figure did not present with any significantly differentially expressed genes. Comparisons with significant differential gene expression included only uncoated control vs APTES at 11 weeks. Gray points indicate genes with no significant difference in the comparison, black points (above the red dashed line) were significant. $N = 3$ for each group.

protective factor prosaposin, which induces endocytosis following ligand binding.[61] While *Gstp1* has also been reported to prevent sepsis-related inflammation,[62] it has also been shown that increased *Gstp1* expression is a cellular responses to oxidative stress or proinflammatory stimuli.[63] Finally, *Sirt2* has been shown to inhibit the transcription of pro-inflammatory genes[64] and inhibit growth cone collapse and neurite outgrowth.[65,66] Taken together, at 11 weeks postimplantation, we found that when APTES-coated devices are compared to uncoated control devices, both demonstrated increased expression levels of genes that could be advantageous and detrimental to microelectrode performance and tissue integration. Neither substrate demonstrates a neuroinflammatory response that would be promising for tissue integration and long-term microelectrode recording performance, and thus, in this case, gene expression results are unable to provide correlative insight into the ability to maintain single unit recordings.

4. CONCLUSIONS

Surface modification by APTES alone does not improve the chronic recording performance of MEAs in vivo but may be beneficial in acute experiments. We observed an initial benefit to the proportion of active electrodes and V_{pp} in the APTES coated group as well as a sustained decrease in noise levels. However, the recording performance of APTES coated devices declined at a faster rate than uncoated devices as evidenced by linear regression and differences in the proportion of active electrode sites at chronic time points. We have not been able to associate these failures with device degradation through electrochemical methods; therefore, it is likely that the observed increase in neuroinflammation plays a role in these failures. Robust analysis of 152 genes associated with neuroinflammatory mechanisms suggested neither the control nor APTES coated probes would provide chronically stable recordings. Together, our work has implications for future studies that might make use of APTES to enable surface modification with bioactive molecules. Based on our observations, any chronic improvement detected from a modified surface enabled by APTES is unlikely to be attributable to incomplete biomolecule deposition since APTES alone is detrimental to the long-term recording performance of intracortical MEAs.

■ ASSOCIATED CONTENT

Supporting Information

The Supporting Information is available free of charge at https://pubs.acs.org/doi/10.1021/acsabm.3c01014.

Reactive amine functionalized microelectrode arrays providing short-term benefit but long-term detriment to in vivo recording performance (Table S1 and Figures S1 and S2) (PDF)

■ AUTHOR INFORMATION

Corresponding Authors

Joseph J. Pancrazio − *Department of Bioengineering, The University of Texas at Dallas, Richardson, Texas 75080, United States*; Email: joseph.pancrazio@utdallas.edu

Jeffrey R. Capadona − *Department of Biomedical Engineering, Case Western Reserve University. 10900 Euclid Ave, Cleveland, Ohio 44106, United States; Advanced Platform Technology Center, Louis Stokes Cleveland Veterans Affairs Medical Center, Cleveland, Ohio 44106, United States;* orcid.org/0000-0001-8030-6947; Email: jrc35@case.edu

Authors

Brandon S. Sturgill − *Department of Bioengineering, The University of Texas at Dallas, Richardson, Texas 75080, United States;* orcid.org/0000-0002-8161-9723

Ana G. Hernandez-Reynoso − *Department of Bioengineering, The University of Texas at Dallas, Richardson, Texas 75080, United States*

Lindsey N. Druschel − *Department of Biomedical Engineering, Case Western Reserve University. 10900 Euclid Ave, Cleveland, Ohio 44106, United States; Advanced Platform Technology Center, Louis Stokes Cleveland Veterans Affairs Medical Center, Cleveland, Ohio 44106, United States*

Thomas J. Smith − *School of Behavioral and BrainSciences, The University of Texas at Dallas, Richardson, Texas 75080, United States*

Pierce E. Boucher − *Department of Biomedical Engineering, Case Western Reserve University. 10900 Euclid Ave, Cleveland, Ohio 44106, United States; Advanced Platform Technology Center, Louis Stokes Cleveland Veterans Affairs Medical Center, Cleveland, Ohio 44106, United States*

George F. Hoeferlin − *Department of Biomedical Engineering, Case Western Reserve University. 10900 Euclid Ave, Cleveland, Ohio 44106, United States; Advanced Platform Technology Center, Louis Stokes Cleveland Veterans Affairs Medical Center, Cleveland, Ohio 44106, United States*

Teresa Thuc Doan Thai − *Department of Bioengineering, The University of Texas at Dallas, Richardson, Texas 75080, United States*

Madison S. Jiang − *School of Behavioral and BrainSciences, The University of Texas at Dallas, Richardson, Texas 75080, United States*

https://doi.org/10.1021/acsabm.3c01014
ACS Appl. Bio Mater. 2024, 7, 1052−1063

Jordan L. Hess − *School of Behavioral and BrainSciences, The University of Texas at Dallas, Richardson, Texas 75080, United States;* orcid.org/0009-0000-4467-3803
Neeha N. Alam − *Department of Bioengineering, The University of Texas at Dallas, Richardson, Texas 75080, United States*
Dhariyat M. Menendez − *Department of Biomedical Engineering, Case Western Reserve University. 10900 Euclid Ave, Cleveland, Ohio 44106, United States; Advanced Platform Technology Center, Louis Stokes Cleveland Veterans Affairs Medical Center, Cleveland, Ohio 44106, United States*
Jonathan L. Duncan − *Department of Biomedical Engineering, Case Western Reserve University. 10900 Euclid Ave, Cleveland, Ohio 44106, United States; Advanced Platform Technology Center, Louis Stokes Cleveland Veterans Affairs Medical Center, Cleveland, Ohio 44106, United States*
Stuart F. Cogan − *Department of Bioengineering, The University of Texas at Dallas, Richardson, Texas 75080, United States*

Complete contact information is available at: https://pubs.acs.org/10.1021/acsabm.3c01014

Author Contributions

[⊥]Equally contributing authors.

Notes

The contents do not represent the views of the U.S. Department of Veterans Affairs, the National Institutes of Health, or the United States Government.
The authors declare no competing financial interest.
All animal care, handling and procedures were performed in compliance ARRIVE guidelines and National Research Council's Guide for the Care and Use of Laboratory Animals. Protocols were approved by the Institutional Animal Care and Use Committees (IACUC) at Louis Stokes Cleveland Department of Veterans Affairs Medical Center and the University of Texas at Dallas.

■ ACKNOWLEDGMENTS

This work was supported in part by the National Institutes of Health, National Institute for Neurological Disorders and Stroke (R01NS110823, GRANT12635723, Capadona/Pancrazio) diversity supplement (Hernandez-Reynoso), and the National Institute for Biomedical Imaging and Bioengineering, (T32EB004314, Capadona/Kirsch). Additional support was provided by Merit Review Award (GRANT12418820, Capadona) and a Senior Research Career Scientist Award (GRANT12635707, Capadona) from the United States (US) Department of Veterans Affairs Rehabilitation Research and Development Service. The authors thank Dr. Alexandra Joshi-Imre and Dr. Negar Geramifard for the fabrication of nonfunctional devices for implantation. Data is available upon request to corresponding author.

■ REFERENCES

(1) Collinger, J. L.; Gaunt, R. A.; Schwartz, A. B. Progress towards restoring upper limb movement and sensation through intracortical brain-computer interfaces. *Current Opinion in Biomedical Engineering* **2018**, *8*, 84−92.
(2) Decramer, T.; Premereur, E.; Zhu, Q.; Van Paesschen, W.; van Loon, J.; Vanduffel, W.; Taubert, J.; Janssen, P.; Theys, T. Single-Unit Recordings Reveal the Selectivity of a Human Face Area. *J. Neurosci.* **2021**, *41* (45), 9340−9349. From NLM Medline.
(3) Weiss, S. A.; Banks, G. P.; McKhann, G. M.; Goodman, R. R.; Emerson, R. G.; Trevelyan, A. J.; Schevon, C. A. Ictal high frequency oscillations distinguish two types of seizure territories in humans. *Brain* **2013**, *136* (12), 3796−3808. From NLM Medline.
(4) Steinmetz, N. A.; Aydin, C.; Lebedeva, A.; Okun, M.; Pachitariu, M.; Bauza, M.; Beau, M.; Bhagat, J.; Bohm, C.; Broux, M.; Chen, S.; Colonell, J.; Gardner, R. J.; Karsh, B.; Kloosterman, F.; Kostadinov, D.; Mora-Lopez, C.; O'Callaghan, J.; Park, J.; Putzeys, J.; Sauerbrei, B.; van Daal, R. J. J.; Vollan, A. Z.; Wang, S.; Welkenhuysen, M.; Ye, Z.; Dudman, J. T.; Dutta, B.; Hantman, A. W.; Harris, K. D.; Lee, A. K.; Moser, E. I.; O'Keefe, J.; Renart, A.; Svoboda, K.; Hausser, M.; Haesler, S.; Carandini, M.; Harris, T. D. Neuropixels 2.0: A miniaturized high-density probe for stable, long-term brain recordings. *Science* **2021**, *372* (6539), No. eabf4588. From NLM Medline.
(5) Jorfi, M.; Skousen, J. L.; Weder, C.; Capadona, J. R. Progress towards biocompatible intracortical microelectrodes for neural interfacing applications. *J. Neural Eng.* **2015**, *12* (1), No. 011001.
(6) Usoro, J. O.; Sturgill, B. S.; Musselman, K. C.; Capadona, J. R.; Pancrazio, J. J. Intracortical Microelectrode Array Unit Yield under Chronic Conditions: A Comparative Evaluation. *Micromachines* **2021**, *12* (8), 972.
(7) Barrese, J. C.; Aceros, J.; Donoghue, J. P. Scanning electron microscopy of chronically implanted intracortical microelectrode arrays in non-human primates. *J. Neural Eng.* **2016**, *13* (2), No. 026003. From NLM Medline.
(8) Prasad, A.; Xue, Q. S.; Dieme, R.; Sankar, V.; Mayrand, R. C.; Nishida, T.; Streit, W. J.; Sanchez, J. C. Abiotic-biotic characterization of Pt/Ir microelectrode arrays in chronic implants. *Front Neuroeng* **2014**, *7*, 2. From NLM PubMed-not-MEDLINE.
(9) Ereifej, E. S.; Rial, G. M.; Hermann, J. K.; Smith, C. S.; Meade, S. M.; Rayyan, J. M.; Chen, K.; Feng, H.; Capadona, J. R. Implantation of Neural Probes in the Brain Elicits Oxidative Stress. *Front Bioeng Biotechnol* **2018**, *6*, 9. From NLM PubMed-not-MEDLINE.
(10) Jeakle, E. N.; Abbott, J. R.; Usoro, J. O.; Wu, Y.; Haghighi, P.; Radhakrishna, R.; Sturgill, B. S.; Nakajima, S.; Thai, T. T. D.; Pancrazio, J. J.; Cogan, S. F.; Hernandez-Reynoso, A. G. Chronic Stability of Local Field Potentials Using Amorphous Silicon Carbide Microelectrode Arrays Implanted in the Rat Motor Cortex. *Micromachines* **2023**, *14* (3), 680.
(11) Patel, P. R.; Zhang, H.; Robbins, M. T.; Nofar, J. B.; Marshall, S. P.; Kobylarek, M. J.; Kozai, T. D.; Kotov, N. A.; Chestek, C. A. Chronic in vivo stability assessment of carbon fiber microelectrode arrays. *J. Neural Eng.* **2016**, *13* (6), No. 066002. From NLM Medline.
(12) Stiller, A. M.; Usoro, J. O.; Lawson, J.; Araya, B.; González-González, M. A.; Danda, V. R.; Voit, W. E.; Black, B. J.; Pancrazio, J. J. Mechanically Robust, Softening Shape Memory Polymer Probes for Intracortical Recording. *Micromachines* **2020**, *11* (6), 619.
(13) Ferguson, M.; Sharma, D.; Ross, D.; Zhao, F. A Critical Review of Microelectrode Arrays and Strategies for Improving Neural Interfaces. *Adv. Healthc Mater.* **2019**, *8* (19), No. e1900558. From NLM Medline.
(14) Boehler, C.; Kleber, C.; Martini, N.; Xie, Y.; Dryg, I.; Stieglitz, T.; Hofmann, U. G.; Asplund, M. Actively controlled release of Dexamethasone from neural microelectrodes in a chronic in vivo study. *Biomaterials* **2017**, *129*, 176−187. From NLM Medline.
(15) Kozai, T. D. Y.; Jaquins-Gerstl, A. S.; Vazquez, A. L.; Michael, A. C.; Cui, X. T. Dexamethasone retrodialysis attenuates microglial response to implanted probes in vivo. *Biomaterials* **2016**, *87*, 157−169. From NLM Medline.
(16) Nguyen, J. K.; Jorfi, M.; Buchanan, K. L.; Park, D. J.; Foster, E. J.; Tyler, D. J.; Rowan, S. J.; Weder, C.; Capadona, J. R. Influence of resveratrol release on the tissue response to mechanically adaptive cortical implants. *Acta Biomater* **2016**, *29*, 81−93. From NLM Medline.
(17) Hoeferlin, G. F.; Bajwa, T.; Olivares, H.; Zhang, J.; Druschel, L. N.; Sturgill, B. S.; Sobota, M.; Boucher, P.; Duncan, J.; Hernandez-Reynoso, A. G.; Cogan, S. F.; Pancrazio, J. J.; Capadona, J. R. Antioxidant Dimethyl Fumarate Temporarily but Not Chronically

Improves Intracortical Microelectrode Performance. *Micromachines* **2023**, *14* (10), 1902.
(18) Rennaker, R. L.; Miller, J.; Tang, H.; Wilson, D. A. Minocycline increases quality and longevity of chronic neural recordings. *J. Neural Eng.* **2007**, *4* (2), L1−5.
(19) Zhong, Y.; Bellamkonda, R. V. Dexamethasone-coated neural probes elicit attenuated inflammatory response and neuronal loss compared to uncoated neural probes. *Brain Res.* **2007**, *1148*, 15−27. From NLM Medline.
(20) He, W.; McConnell, G. C.; Bellamkonda, R. V. Nanoscale laminin coating modulates cortical scarring response around implanted silicon microelectrode arrays. *J. Neural Eng.* **2006**, *3* (4), 316−326. From NLM Medline.
(21) Sridar, S.; Churchward, M. A.; Mushahwar, V. K.; Todd, K. G.; Elias, A. L. Peptide modification of polyimide-insulated microwires: Towards improved biocompatibility through reduced glial scarring. *Acta Biomater* **2017**, *60*, 154−166. From NLM Medline.
(22) Richardson, R. T.; Wise, A. K.; Thompson, B. C.; Flynn, B. O.; Atkinson, P. J.; Fretwell, N. J.; Fallon, J. B.; Wallace, G. G.; Shepherd, R. K.; Clark, G. M.; O'Leary, S. J. Polypyrrole-coated electrodes for the delivery of charge and neurotrophins to cochlear neurons. *Biomaterials* **2009**, *30* (13), 2614−2624. From NLM Medline.
(23) Potter, K. A.; Jorfi, M.; Householder, K. T.; Foster, E. J.; Weder, C.; Capadona, J. R. Curcumin-releasing mechanically adaptive intracortical implants improve the proximal neuronal density and blood-brain barrier stability. *Acta Biomater* **2014**, *10* (5), 2209−2222. From NLM Medline.
(24) Hernandez-Reynoso, A. G.; Sturgill, B. S.; Hoeferlin, G. F.; Druschel, L. N.; Krebs, O. K.; Menendez, D. M.; Thai, T. T. D.; Smith, T. J.; Duncan, J.; Zhang, J.; Mittal, G.; Radhakrishna, R.; Desai, M. S.; Cogan, S. F.; Pancrazio, J. J.; Capadona, J. R. The effect of a Mn(III)tetrakis(4-benzoic acid)porphyrin (MnTBAP) coating on the chronic recording performance of planar silicon intracortical microelectrode arrays. *Biomaterials* **2023**, *303*, No. 122351. From NLM Medline.
(25) Eles, J. R.; Vazquez, A. L.; Snyder, N. R.; Lagenaur, C.; Murphy, M. C.; Kozai, T. D.; Cui, X. T. Neuroadhesive L1 coating attenuates acute microglial attachment to neural electrodes as revealed by live two-photon microscopy. *Biomaterials* **2017**, *113*, 279−292. From NLM Medline.
(26) Golabchi, A.; Woeppel, K. M.; Li, X.; Lagenaur, C. F.; Cui, X. T. Neuroadhesive protein coating improves the chronic performance of neuroelectronics in mouse brain. *Biosens Bioelectron* **2020**, *155*, No. 112096. From NLM Medline.
(27) Azemi, E.; Lagenaur, C. F.; Cui, X. T. The surface immobilization of the neural adhesion molecule L1 on neural probes and its effect on neuronal density and gliosis at the probe/tissue interface. *Biomaterials* **2011**, *32* (3), 681−692. From NLM Medline.
(28) Zheng, X. S.; Snyder, N. R.; Woeppel, K.; Barengo, J. H.; Li, X.; Eles, J.; Kolarcik, C. L.; Cui, X. T. A superoxide scavenging coating for improving tissue response to neural implants. *Acta Biomater* **2019**, *99*, 72−83. From NLM Medline.
(29) Sypabekova, M.; Hagemann, A.; Rho, D.; Kim, S. Review: 3-Aminopropyltriethoxysilane (APTES) Deposition Methods on Oxide Surfaces in Solution and Vapor Phases for Biosensing Applications. *Biosensors* **2023**, *13* (1), 36.
(30) Wolf, N. R.; Rai, P.; Glass, M.; Milos, F.; Maybeck, V.; Offenhausser, A.; Wordenweber, R. Mechanical and Electronic Cell-Chip Interaction of APTES-Functionalized Neuroelectronic Interfaces. *ACS Appl. Bio Mater.* **2021**, *4* (8), 6326−6337. From NLM Medline.
(31) Potter-Baker, K. A.; Nguyen, J. K.; Kovach, K. M.; Gitomer, M. M.; Srail, T. W.; Stewart, W. G.; Skousen, J. L.; Capadona, J. R. Development of Superoxide Dismutase Mimetic Surfaces to Reduce Accumulation of Reactive Oxygen Species for Neural Interfacing Applications. *J. Mater. Chem. B* **2014**, *2* (16), 2248−2258.
(32) Harpaz, D.; Koh, B.; Seet, R. C. S.; Abdulhalim, I.; Tok, A. I. Y. Functionalized silicon dioxide self-referenced plasmonic chip as point-of-care biosensor for stroke biomarkers NT-proBNP and S100beta. *Talanta* **2020**, *212*, No. 120792. From NLM Medline.
(33) Bodur, O. C.; Dinc, S.; Ozmen, M.; Arslan, F. A sensitive amperometric detection of neurotransmitter acetylcholine using carbon dot-modified carbon paste electrode. *Biotechnol Appl. Biochem* **2021**, *68* (1), 20−29. From NLM Medline.
(34) Puri, N.; Sharma, V.; Tanwar, V. K.; Singh, N.; Biradar, A. M.; Rajesh. Enzyme-modified indium tin oxide microelectrode array-based electrochemical uric acid biosensor. *Prog. Biomater* **2013**, *2* (1), 5. From NLM PubMed-not-MEDLINE.
(35) Kuddannaya, S.; Bao, J.; Zhang, Y. Enhanced In Vitro Biocompatibility of Chemically Modified Poly(dimethylsiloxane) Surfaces for Stable Adhesion and Long-term Investigation of Brain Cerebral Cortex Cells. *ACS Appl. Mater. Interfaces* **2015**, *7* (45), 25529−25538. From NLM Medline.
(36) Luong, J. H. T.; Hrapovic, S.; Wang, D. S. Multiwall carbon nanotube (MWCNT) based electrochemical biosensors for mediator-less detection of putrescine. *Electroanal* **2005**, *17* (1), 47−53.
(37) Pardo-Figuerez, M.; Martin, N. R. W.; Player, D. J.; Capel, A. J.; Christie, S. D. R.; Lewis, M. P. Neural and Aneural Regions Generated by the Use of Chemical Surface Coatings. *ACS Biomater Sci. Eng.* **2018**, *4* (1), 98−106. From NLM PubMed-not-MEDLINE.
(38) Sruthi, S.; Loiseau, A.; Boudon, J.; Sallem, F.; Maurizi, L.; Mohanan, P. V.; Lizard, G.; Millot, N. In vitro interaction and biocompatibility of titanate nanotubes with microglial cells. *Toxicol. Appl. Pharmacol.* **2018**, *353*, 74−86. From NLM Medline.
(39) Borah, R.; Ingavle, G. C.; Sandeman, S. R.; Kumar, A.; Mikhalovsky, S. V. Amine-Functionalized Electrically Conductive Core-Sheath MEH-PPV:PCL Electrospun Nanofibers for Enhanced Cell-Biomaterial Interactions. *ACS Biomater Sci. Eng.* **2018**, *4* (9), 3327−3346. From NLM PubMed-not-MEDLINE.
(40) He, W.; Bellamkonda, R. V. Nanoscale neuro-integrative coatings for neural implants. *Biomaterials* **2005**, *26* (16), 2983−2990. From NLM Medline.
(41) Faucheux, N.; Schweiss, R.; Lutzow, K.; Werner, C.; Groth, T. Self-assembled monolayers with different terminating groups as model substrates for cell adhesion studies. *Biomaterials* **2004**, *25* (14), 2721−2730. From NLM Medline.
(42) Kleinfeld, D.; Kahler, K. H.; Hockberger, P. E. Controlled outgrowth of dissociated neurons on patterned substrates. *J. Neurosci.* **1988**, *8* (11), 4098−4120. From NLM Medline.
(43) Wolf, N. R.; Yuan, X.; Hassani, H.; Milos, F.; Mayer, D.; Breuer, U.; Offenhausser, A.; Wordenweber, R. Surface Functionalization of Platinum Electrodes with APTES for Bioelectronic Applications. *ACS Appl. Bio Mater.* **2020**, *3* (10), 7113−7121. From NLM PubMed-not-MEDLINE.
(44) Markov, A.; Maybeck, V.; Wolf, N.; Mayer, D.; Offenhäusser, A.; Wördenweber, R. Engineering of Neuron Growth and Enhancing Cell-Chip Communication via Mixed SAMs. *ACS Appl. Mater. Interfaces* **2018**, *10* (22), 18507−18514.
(45) Cogan, S. F. Neural stimulation and recording electrodes. *Annu. Rev. Biomed Eng.* **2008**, *10*, 275−309. From NLM Medline.
(46) Krebs, O. K.; Mittal, G.; Ramani, S.; Zhang, J.; Shoffstall, A. J.; Cogan, S. F.; Pancrazio, J. J.; Capadona, J. R. Tools for Surface Treatment of Silicon Planar Intracortical Microelectrodes. *J. Vis Exp* **2022**, *184*, No. e63500. From NLM Medline.
(47) Sturgill, B.; Radhakrishna, R.; Thai, T. T. D.; Patnaik, S. S.; Capadona, J. R.; Pancrazio, J. J. Characterization of Active Electrode Yield for Intracortical Arrays: Awake versus Anesthesia. *Micromachines (Basel)* **2022**, *13* (3), 480. From NLM PubMed-not-MEDLINE.
(48) Potter, K. A.; Buck, A. C.; Self, W. K.; Capadona, J. R. Stab injury and device implantation within the brain results in inversely multiphasic neuroinflammatory and neurodegenerative responses. *J. Neural Eng.* **2012**, *9* (4), No. 046020. From NLM Medline.
(49) Song, S.; Druschel, L. N.; Chan, E. R.; Capadona, J. R. Differential expression of genes involved in the chronic response to intracortical microelectrodes. *Acta Biomater* **2023**, *169*, 348−362. From NLM Medline.

https://doi.org/10.1021/acsabm.3c01014
ACS Appl. Bio Mater. 2024, 7, 1052−1063

(50) Song, S.; Regan, B.; Ereifej, E. S.; Chan, E. R.; Capadona, J. R. Neuroinflammatory Gene Expression Analysis Reveals Pathways of Interest as Potential Targets to Improve the Recording Performance of Intracortical Microelectrodes. *Cells* **2022**, *11* (15), 2348. From NLM Medline.
(51) Bedell, H. W.; Schaub, N. J.; Capadona, J. R.; Ereifej, E. S. Differential expression of genes involved in the acute innate immune response to intracortical microelectrodes. *Acta Biomater* **2020**, *102*, 205−219. From NLM Medline.
(52) Motulsky, H. J.; Brown, R. E. Detecting outliers when fitting data with nonlinear regression - a new method based on robust nonlinear regression and the false discovery rate. *BMC Bioinformatics* **2006**, *7*, 123. From NLM Medline.
(53) Prasad, A.; Sanchez, J. C. Quantifying long-term microelectrode array functionality using chronic in vivo impedance testing. *J. Neural Eng.* **2012**, *9* (2), No. 026028. From NLM Medline.
(54) Neto, J. P.; Baiao, P.; Lopes, G.; Frazao, J.; Nogueira, J.; Fortunato, E.; Barquinha, P.; Kampff, A. R. Does Impedance Matter When Recording Spikes With Polytrodes? *Front Neurosci* **2018**, *12*, 715. From NLM PubMed-not-MEDLINE.
(55) Urdaneta, M. E.; Kunigk, N. G.; Penaloza-Aponte, J. D.; Currlin, S.; Malone, I. G.; Fried, S. I.; Otto, K. J. Layer-dependent stability of intracortical recordings and neuronal cell loss. *Front Neurosci* **2023**, *17*, No. 1096097. From NLM PubMed-not-MEDLINE.
(56) Cai, S.; Wu, C.; Yang, W.; Liang, W.; Yu, H.; Liu, L. Recent advance in surface modification for regulating cell adhesion and behaviors. *Nanotechnol. Rev.* **2020**, *9* (1), 971−989.
(57) Kowianski, P.; Lietzau, G.; Czuba, E.; Waskow, M.; Steliga, A.; Morys, J. BDNF: A Key Factor with Multipotent Impact on Brain Signaling and Synaptic Plasticity. *Cell Mol. Neurobiol* **2018**, *38* (3), 579−593. From NLM Medline.
(58) Li, C. X.; Wang, J. S.; Wang, W. N.; Xu, D. K.; Zhou, Y. T.; Sun, F. Z.; Li, Y. Q.; Guo, F. Z.; Ma, J. L.; Zhang, X. Y.; Chang, M. J.; Xu, B. H.; Ma, F.; Qian, H. L. Expression dynamics of periodic transcripts during cancer cell cycle progression and their correlation with anticancer drug sensitivity. *Mil Med. Res.* **2022**, *9* (1), 71. From NLM Medline.
(59) Yanagisawa, K.; Konishi, H.; Arima, C.; Tomida, S.; Takeuchi, T.; Shimada, Y.; Yatabe, Y.; Mitsudomi, T.; Osada, H.; Takahashi, T. Novel metastasis-related gene CIM functions in the regulation of multiple cellular stress-response pathways. *Cancer Res.* **2010**, *70* (23), 9949−9958. From NLM Medline.
(60) Vantaggiato, C.; Redaelli, F.; Falcone, S.; Perrotta, C.; Tonelli, A.; Bondioni, S.; Morbin, M.; Riva, D.; Saletti, V.; Bonaglia, M. C.; Giorda, R.; Bresolin, N.; Clementi, E.; Bassi, M. T. A novel CLN8 mutation in late-infantile-onset neuronal ceroid lipofuscinosis (LINCL) reveals aspects of CLN8 neurobiological function. *Hum Mutat* **2009**, *30* (7), 1104−1116. From NLM Medline.
(61) Meyer, R. C.; Giddens, M. M.; Schaefer, S. A.; Hall, R. A. GPR37 and GPR37L1 are receptors for the neuroprotective and glioprotective factors prosaptide and prosaposin. *Proc. Natl. Acad. Sci. U. S. A.* **2013**, *110* (23), 9529−9534. From NLM Medline.
(62) Zhou, Y.; Cao, X.; Yang, Y.; Wang, J.; Yang, W.; Ben, P.; Shen, L.; Cao, P.; Luo, L.; Yin, Z. Glutathione S-Transferase Pi Prevents Sepsis-Related High Mobility Group Box-1 Protein Translocation and Release. *Front Immunol* **2018**, *9*, 268. From NLM Medline.
(63) Luo, L.; Wang, Y.; Feng, Q.; Zhang, H.; Xue, B.; Shen, J.; Ye, Y.; Han, X.; Ma, H.; Xu, J.; Chen, D.; Yin, Z. Recombinant protein glutathione S-transferases P1 attenuates inflammation in mice. *Mol. Immunol* **2009**, *46* (5), 848−857. From NLM Medline.
(64) Rothgiesser, K. M.; Erener, S.; Waibel, S.; Luscher, B.; Hottiger, M. O. SIRT2 regulates NF-kappaB dependent gene expression through deacetylation of p65 Lys310. *J. Cell Sci.* **2010**, *123* (24), 4251−4258. From NLM Medline.
(65) Pandithage, R.; Lilischkis, R.; Harting, K.; Wolf, A.; Jedamzik, B.; Luscher-Firzlaff, J.; Vervoorts, J.; Lasonder, E.; Kremmer, E.; Knoll, B.; Luscher, B. The regulation of SIRT2 function by cyclin-dependent kinases affects cell motility. *J. Cell Biol.* **2008**, *180* (5), 915−929. From NLM Medline.
(66) Jeong, S. G.; Cho, G. W. The tubulin deacetylase sirtuin-2 regulates neuronal differentiation through the ERK/CREB signaling pathway. *Biochem. Biophys. Res. Commun.* **2017**, *482* (1), 182−187. From NLM Medline.

https://doi.org/10.1021/acsabm.3c01014
ACS Appl. Bio Mater. 2024, 7, 1052−1063